Journal of Structural Geology 35 (2012) 64–77

Contents lists available at SciVerse ScienceDirect

Journal of Structural Geology

journal homepage: www.elsevier.com/locate/jsg

Integrated estimates of the thickness of the fault damage zone in granitic terrain based on penetrative mesocracks and XRD analyses of quartz

Hideo Takagi [a,*], Kazuhiro Takahashi [b,1], Koji Shimada [c], Kosuke Tsutsui [b], Reiko Miura [d], Narumi Kato [d,2], Shigeru Takizawa [e]

[a] Faculty of Education and Integrated Arts and Sciences, Waseda University, Tokyo 169-8050, Japan
[b] Graduate School of Creative Science and Engineering, Waseda University, Shinjuku 169-8050, Japan
[c] Japan Atomic Energy Agency, FBR Monju, Tsuruga, Fukui 919-1279, Japan
[d] Department of Earth Sciences, School of Education, Waseda University, Tokyo 169-8050, Japan
[e] Institute of Geoscience, University of Tsukuba, Ibaraki 305-8572, Japan

ARTICLE INFO

Article history:
Received 27 February 2011
Received in revised form
31 October 2011
Accepted 17 November 2011
Available online 4 December 2011

Keywords:
Cataclastic zone
Mesocrack density
X-ray line broadening
Quartz crystallinity index
Median Tectonic Line
Atotsugawa Fault

ABSTRACT

We estimated the thickness of the fault damage zone in granitoid along the Iinan transect at the Median Tectonic Line (MTL) and along the Magawa transect at the Atotsugawa Fault, southwest Japan, based on the density of penetrative mesocracks, and on analyses of intracrystalline strain in pulverized quartz using X-ray line broadening (β) and the crystallinity index (CI). The mesocrack density and intracrystalline strain show an increase toward the MTL, from ~400 m from the fault. High amounts of intracrystalline strain in quartz, characterized by large β and low CI, reflect the presence of dense, heterogeneous tangles of short dislocations. For the Atotsugawa Fault, in contrast, we observed no increase in intracrystalline strain within quartz, even within highly fractured rock showing high mesocrack density located close to the fault (~10 m). This difference in the intensity of intracrystalline strain close to the fault between the MTL and the Atotsugawa Fault suggests that dislocation substructures did not accumulate at shallower levels in the brittle regime, but accumulated at deeper levels. Accordingly, analyses of intracrystalline strain in pulverized quartz, using X-ray line broadening and CI are useful in evaluating the degree of cataclasis of quartz-bearing rocks at deeper levels of the brittle regime.

1. Introduction

The thickness of a brittle fault zone is an important parameter in estimating fault length, total displacement, and the history of fault activity (e.g., Wibberley et al., 2010). These factors are critical in selecting sites for the disposal of radioactive waste in relation to water pathways and in evaluating rock strength, especially at sites located close to faults in the field of engineering geology. Estimates of the thickness of a brittle fault zone (i.e., fault damage zone; Chester and Logan, 1986; Kim et al., 2004), including the cataclastic zone, have been undertaken as part of evaluating the geological strength index in engineering geology (e.g., Marinos et al., 2005), and as evaluating the density and orientation of meso- or microcracks with respect to distance from the fault (Anders and Wiltschko, 1994; Kanaori, 2001; Lin et al., 2001; Wilson et al., 2003; Berg and Skar, 2005; Micarelli et al., 2006). The intensity of cataclasis has been determined based on microscopic criteria (e.g., Takagi, 1983), and the thickness of the cataclastic zone in granitic terrain along the Median Tectonic Line (MTL) in southwest Japan has been estimated to be 200–300 m (Takagi, 1983, 1985).

Dislocation density in quartz grains has been estimated based on analyses of intracrystalline strain using X-ray line broadening of the 110, 220, and 330 peaks of pulverized quartz (Aikawa and Aoyama, 1983; Nagao and Aikawa, 1983, 1985). Such analyses have been performed for quartz grains in a cataclastic zone (Ui et al., 1988) using the crystallinity index (CI) for quartz introduced by Murata and Norman (1976). Takagi et al. (1988) estimated the intracrystalline strain in quartz for ductile to brittle shear zones in the Late Cretaceous Ryoke granite, Japan, using both X-ray line broadening and CI, revealing little change in intracrystalline strain from the protolith granite to strongly mylonitized granite, whereas an abrupt increase in strain is observed for cataclasite and fault gouge that previously underwent cataclasis at depth.

* Corresponding author.
E-mail address: hideo@waseda.jp (H. Takagi).
[1] Present address: Japan Petroleum Exploration Co. Ltd., Tokyo 100-0005, Japan.
[2] Present address: Editing Department Tokyo Branch, The Shizuoka Shimbun, Tokyo 104-0061, Japan.

0191-8141/$ – see front matter © 2011 Elsevier Ltd. All rights reserved.
doi:10.1016/j.jsg.2011.11.008

In the context of these previous studies, we performed an integrated evaluation of (1) the degree of mylonitization and cataclasis based on microscopic observations, following Takagi (1983, 1985, 1986); (2) mesoscopic crack density using the intercept method; and (3) intracrystalline strain using X-ray line broadening and the CI of pulverized quartz, all with respect to distance from two major faults: the MTL and the Atotsugawa Fault in southwest Japan (Fig. 1). We do not consider non-penetrative macroscopic fractures involving open fractures (mode 1) or faults that are widely spaced along the main fault (although these should be taken into account when considering the true thickness of the fault damage zone), because of the limited exposure and the difficulties encountered in collecting data on such fractures. Therefore, in this paper, the cataclastic zone is defined as the fault damage zone in which mesoscopic penetrative fractures are developed.

We will discuss and compare the thickness of the cataclastic zones for these major faults in granitic terrain. The Ryoke granitic rocks, which occur along the MTL in the study area, record ductile deformation overprinted by brittle shear deformation (from deeper to near-surface crustal levels) from the Late Cretaceous, with no evidence of active (Quaternary) faulting. Isotopic age data obtained for brittle fault rocks (e.g., pseudotachylyte: Takagi et al., 2010; fault gouge: Takagi et al., 2005) along the MTL suggest that the brittle deformation took place from the Paleogene (c. 60 Ma). In contrast, the Triassic Hida granitic rocks, located along the Atotsugawa Fault, have experienced only brittle deformation at shallow crustal levels from the Paleogene (c. 60 Ma; Takagi et al., 2005) to the present day.

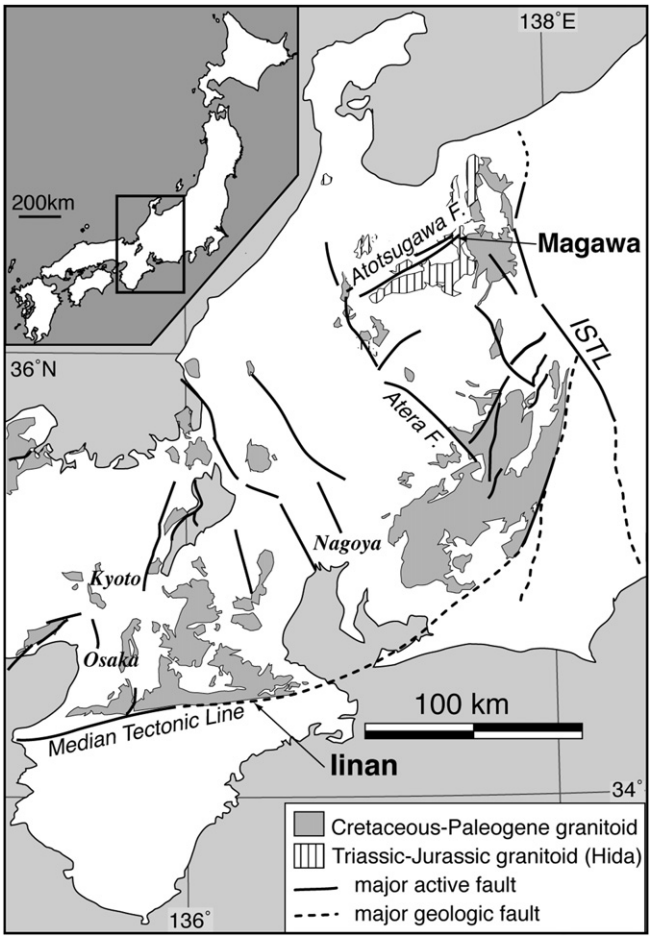

Fig. 1. Index map of the analyzed faults (Median Tectonic Line and Atotsugawa Fault). ISTL: Itoigawa–Shizuoka Tectonic Line.

The difference between these two areas, in terms of spatial variations in mesocrack density and intracrystalline strain with respect to distance from the fault, reflects differences in the deformation history and environment. The aim of this paper is to assess and explain these differences.

2. Geological background

2.1. MTL: The Iinan transect

The MTL is the longest inland fault in Japan, extending for nearly 1000 km from Kanto to Kyushu via Chubu, Kinki, and Shikoku. The MTL separates the low-P/T Ryoke metamorphic belt to the north from the high-P/T Sanbagawa belt to the south. The analyzed samples were collected from the Iinan transect (Fig. 1) in Mié Prefecture, Kinki region, where the Ryoke granitic rocks are in direct contact with the Sanbagawa metamorphic rocks. The orientation of the MTL along the Iinan transect is unaffected by regional bending associated with Miocene arc–arc collision (between the Izu–Ogasawara and Honshu arcs), whereas in the Chubu region the MTL is rotated eastward, striking NE–SW to N–S with a near-vertical dip. The MTL along the Iinan transect strikes N80° E and dips northward at 60–70°. The analyzed samples were collected from the Nishitani River in the south to the Shidehara River in the north, along a 7-km transect oriented normal to the MTL (Fig. 2). The Ryoke rocks in this area are mainly foliated tonalite (Hatai Tonalite) and mafic to intermediate fine-grained banded plutonic rocks (microdiorite–microgabbro). Small, elongate outcrops of augen granodiorite (Yokono Granite) are oriented parallel to the foliation within the tonalite and within the mafic to intermediate rocks. The low-P/T Ryoke metamorphic rocks (pelitic to psammitic gneiss and schist) occur as lenticular bodies in the Hatai Tonalite and are widely exposed in the northernmost part of the study area. Mylonite zones are developed in the Ryoke granitic rocks at ~1 km from the MTL (the Southern Marginal Shear Zone) and at ~3 km from the MTL (the Inner Shear Zone) (Takagi, 1985; Shimada et al., 1998).

Cataclasite is generally only found close to the MTL, although it also occurs in a zone located ~300 m from the fault (Takagi, 1985). Fault gouge is restricted to a layer (several centimeters thick) that occurs along the MTL itself, as observed in outcrops at the Nishitani River (Takagi, 1985). The study area is cut by E–W-trending faults (the Nyunomata, Shidehara, Minamata, and Hiyama faults) marked by zones of intense alteration. Shimada et al. (2001) reported pseudotachylyte from the MTL in the Taki area (Mié Prefecture), east of the Iinan area. The initiation of brittle deformation along the MTL occurred at 60 Ma, based on fission track dating of pseudotachylyte from the Taki area (Takagi et al., 2010).

The Hatai Tonalite is a foliated medium- to coarse-grained hornblende biotite tonalite that consists of plagioclase, quartz, hornblende, biotite, minor K-feldspar, and accessory titanite, apatite, zircon, and epidote. Biotite is altered to chlorite, and plagioclase is altered to sericite or saussurite. The foliation is folded, defining E–W-trending kilometer-scale synform–antiform pair (Fig. 2). Within ~2 km of the MTL, the mylonitic foliation strikes between N80° E and E–W, dipping at 60°–80° to the north. An ultramylonite zone occurs within ~200 m from the MTL, overprinted by cataclasis (Takagi, 1985; Shimada et al., 1998). K–Ar geochronology data for the Hatai Tonalite yield ages of 73–84 Ma (hornblende) and 68–70 Ma (biotite) (Takagi et al., 1989).

The Yokono Granodiorite is a coarse-grained foliated granodiorite to granite, characterized by coarse-grained K-feldspar porphyroclasts (augen). The granodiorite is weakly mylonitized and consists of plagioclase, K-feldspar, quartz, biotite, and hornblende, with accessory allanite, titanite, apatite, epidote, and zircon.

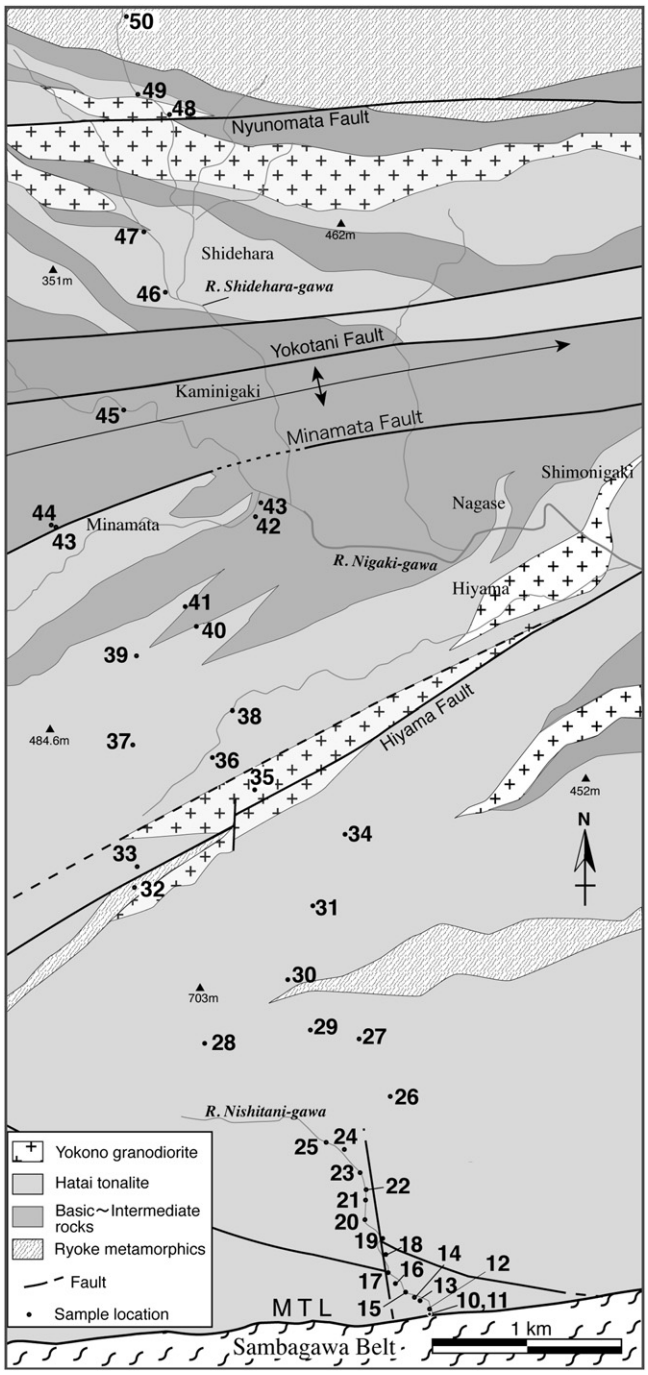

Fig. 2. Geological map of the Ryoke Belt (modified after Takagi, 1985), showing sample locations along the Iinan transect to the north of the MTL.

Fine-grained, banded intermediate to mafic rocks (microdiorite–microgabbro) are composed mainly of plagioclase, quartz, biotite, and hornblende. These rocks are interfingered with the Hatai Tonalite and Yokono Granodiorite at the respective contacts (Takagi, 1985).

Samples for analysis were collected mainly from the Hatai Tonalite body, and to a lesser degree from microdioritic rocks (Fig. 2).

2.2. Atotsugawa Fault: the Magawa transect

The Atotsugawa Fault, which is one of the main dextral active faults in Central Japan, strikes NE–SW along a length of ~64 km in the Hida Mountains (Research Group for Active Faults of Japan, 1991). The fault terminates at active volcanoes (Tateyama in the east and Hakusan in the west) and is marked by a linear trace of minor seismic activity. The average displacement velocity is 3–5 m/1000 yr in the horizontal and ~2.5 m/1000 yr in the vertical (Akahane et al., 2001).

The analyzed samples were collected along the Magawa transect (Fig. 1), at the easternmost part of the fault, where the protolith to the Hida granitic rocks (Triassic) is well exposed. This route contains one of the best exposures of an active fault in Japan, at a site that has been designated a natural monument. Along this route, samples were collected at regular intervals at distances of up to 500 m from the Atotsugawa Fault (Fig. 3).

At the Magawa transect, the Atotsugawa Fault strikes ENE–WSW and dips at 80° to the SSE. The fault separates gneissose medium-grained granodiorite to the north from Quaternary lacustrine and terrace deposits to the south (Fig. 3). On the NW (granitic) side of the fault, the fault core consists of fault breccia and fault gouge in a zone that is ~50 cm thick. The fracture zone within the Hida granite extends to at least 20 m from the fault, and contains a displaced dark-green mafic dyke. Intact granodiorite occurs at distances greater than ~20 m from the fault, although Kanaori et al. (1988), who described in detail the meso- and microstructures in the granite along this route, suggested that brittle deformation structures are seen at up to 100 m from the fault, including minor faults oriented parallel to the Atotsugawa Fault.

On the SE (Quaternary) side of the fault, drag folds of lacustrine deposits are observed within several meters of the fault, and clasts are highly fractured within 20 cm of the fault. A zone of brownish fault gouge (1–2 cm thick) is observed where the fault cuts a terrace deposit. The fault surface in the gouge zone (inset in Fig. 3) contains slickenlines that plunge at 20° toward S60° W, suggesting dextral displacement with a minor, normal dip-slip component. Dark brown, fractured pseudotachylyte occurs within several meters of the fault (Takagi and Takahashi, 2007). The protolith granodiorite is a weakly mylonitized medium-grained leucocratic biotite granodiorite (the Sugodani Granite; Harayama et al., 2000) that consists mainly of quartz, K-feldspar, plagioclase, biotite, minor muscovite and hornblende, and accessory epidote, allanite, apatite, and zircon. The timing of mylonitization of the Hida granitic rocks in this area is considered to be 215–211 Ma, based on SHRIMP zircon dating (Takahashi et al., 2010). Illite within fault gouge at the western part of the Atotsugawa Fault yields a K–Ar age of 61 Ma, which is similar to the oldest age of fault gouge from the active segment of the MTL in Shikoku (Takagi et al., 2005). These age data indicate that the initiation of brittle deformation and hydrothermal alteration occurred in the early Paleogene.

3. Degree of mylonitization and cataclasis

To estimate the density of mesocracks and the amount of intracrystalline strain, we assessed the degree and nature of mylonitization and cataclasis based on microscopic observations. The degree of mylonitization along the MTL is well recorded by the progressive grain-size reduction of recrystallized quartz grains toward the fault (Takagi, 1985, 1986). The trend in grain-size variation (with respect to distance from the MTL) at the Iinan transect has been described by Takagi (1985) and Shimada et al. (1998). The degree of cataclasis can be classified into four categories based on microscopic observations (Takagi, 1983). In this section, we describe spatial trends in the microstructure and fabric of recrystallized quartz with respect to distance from the MTL and from the Atotsugawa Fault.

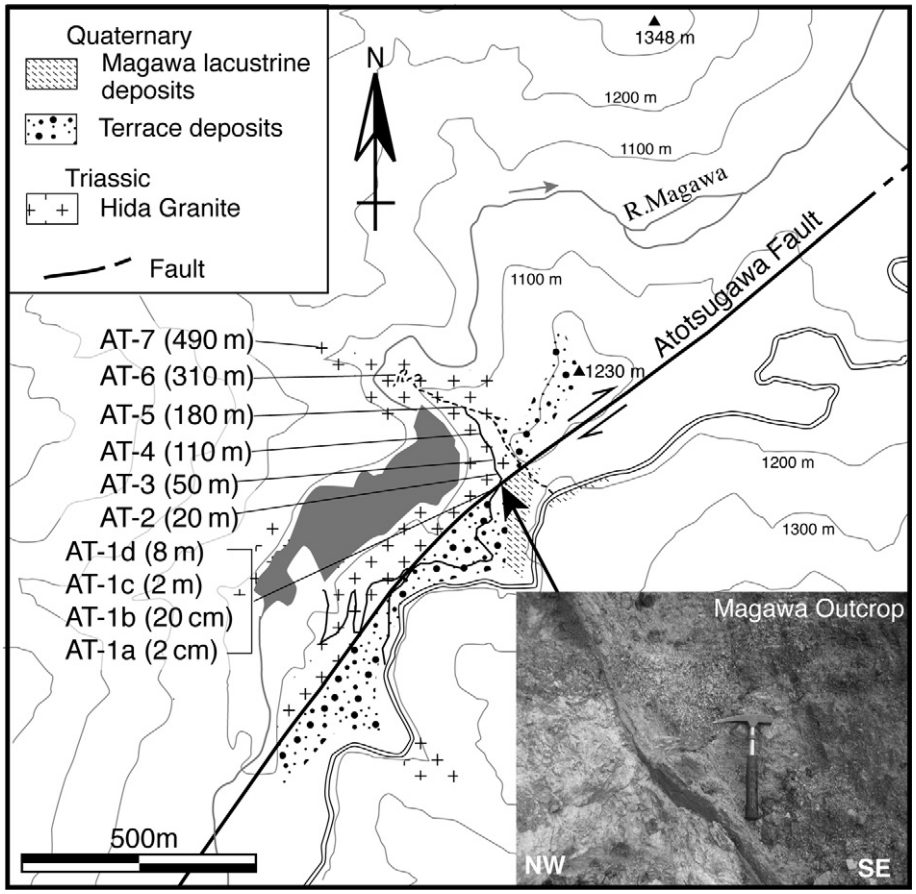

Fig. 3. Sample locations along the Magawa transect, oriented approximately normal to the strike of the Atotsugawa Fault. The inset shows a photograph of the fault (site AT-1a) where it separates the Hida granite (left) from gravel (right).

3.1. Mylonitization

3.1.1. MTL: the Iinan transect

The half-thickness of the mylonite zone along the MTL is ~1 km. The microstructure of quartz in mylonitic rocks at distances of 300–1000 m from the MTL, and at ~3 km (the Inner Shear Zone) is characterized by polygonal aggregates (P-type; Masuda and Fujimura, 1981; Takagi, 1985), and the *c*-axis fabric is characterized by a Y-maximum (or type-II crossed girdle) pattern. At distances of 200–300 m from the MTL, quartz grains have a higher aspect ratio and serrated grain boundaries (S-type; Masuda and Fujimura, 1981; Takagi, 1985), and the *c*-axis fabric is characterized by a pattern between a type-I crossed girdle and a single girdle. Within 200 m of the MTL, quartz grains are very fine-grained, ~10 μm in diameter (F-type; Takagi, 1985), and the rocks are ultramylonite.

This trend in quartz microstructure and fabric toward the MTL indicates that high-T/low-$\dot{\varepsilon}$ (strain rate) deformation extends over a wide area, whereas low-T/high-$\dot{\varepsilon}$ deformation is localized and has been reactivated. Cataclastic deformation is also overprinted on the low-temperature mylonite to ultramylonite (including S-type to F-type quartz grains) at shallower depths. Trends in the grain size of recrystallized quartz will be shown later.

3.1.2. Atotsugawa Fault: the Magawa transect

The Hida granitic rocks (Sugodani Granite) along the Atotsugawa Fault at the Magawa transect are moderately mylonitized and show a porphyroclastic texture, indicating dextral shear. The mylonitic foliation is sub-parallel to the orientation of the Atotsugawa Fault, although the intensity of mylonitization does not increase toward the fault. Therefore, the mylonitization must have preceded the initiation of the Atotsugawa Fault. The mylonite is characterized by quartz ribbons and polygonal aggregates of feldspar, with little undulatory extinction and grain-size reduction.

3.2. Cataclasis

The degree of cataclasis was assessed based on observations of thin sections and classified into the following four types (in order of increasingly intense cataclasis) (Fig. 4):

- A type (uncrushed rocks): No evidence of cataclasis, few fractures or veins (fewer than five fractures or veins in an area of thin section of 3 × 2 cm).
- B type (slightly crushed rocks): No granulation or pulverization, but more than five fractures or veins in an area of thin section of 3 × 2 cm.
- C type (moderately crushed rocks): Partly brecciated and many fractures or veins. In some cases, a narrow pulverized zone occurs (thickness of 100 μm to 2 mm), although other areas retain the texture of the protolith.
- D type (intensively crushed rocks): Brecciation and pulverization is predominant throughout the entire thin section; the rock is classified as protocataclasite and possibly cataclasite.

Table 1 lists data on the degree of cataclasis in each sample from the MTL and from the Atotsugawa Fault.

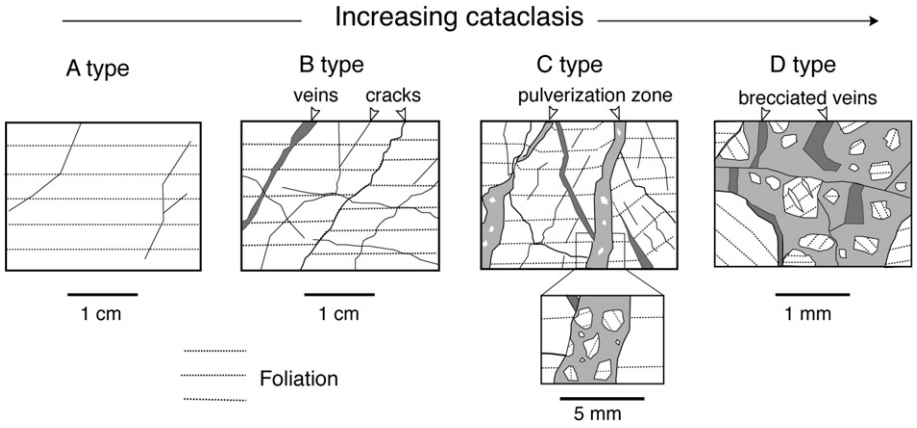

Fig. 4. Relative degree of cataclasis based on observations of thin sections (3.5 × 2.5 cm in area) under the microscope (after Takagi, 1983). A: uncrushed, B: slightly crushed, C: moderately crushed, D: intensively crushed (cataclasite).

3.2.1. MTL: the Iinan transect

In terms of the degree of cataclasis, the samples collected far from the MTL are A or B type, except where collected close to other faults. Samples within 1 km of the MTL are C type, while those within ~300 m of the MTL are C and D type. Close to the fault (within 70 m), the samples are D type (Table 1). The vein minerals near the MTL are mainly calcite and minor chlorite.

3.2.2. Atotsugawa Fault: the Magawa transect

Samples located more than 20 m from the Atotsugawa Fault are mainly A type, whereas those located within 10 m of the fault are C or D type (Table 1). The vein minerals near the fault are mainly calcite.

4. Trends in mesocrack density

We measured the density of mesocracks in oriented, polished rock slabs to estimate the strike-normal thickness of the damage zone along the MTL and the Atotsugawa Fault. The measured mesocracks were all transgranular, because the density of grain-boundary cracks depends on the grain size of the protolith, and intragranular cracks (microcracks) are too small to be measured accurately using the method employed in this study.

4.1. Analytical method

4.1.1. Imaging mesocracks

From oriented samples, we prepared three orthogonal, polished compass-oriented slices: horizontal, vertical oriented N–S, and vertical oriented E–W, because cataclastic rocks along the MTL and the Atotsugawa fault have few structural features such as foliations or lineations. The slabs were polished using #1500 alundum and scanned at 1600 dpi using a standard image scanner. The scanned images were uploaded to a PC in four times magnification on one side (~20 cm) and the cracks were hand-traced in Adobe Illustrator with a line thickness of 1 pt (=0.353 mm). The fault core samples commonly contain fracture zones or mineral veins that are thicker than the mesocracks. In such case, both margins of such zones or veins were traced, along with any internal mesocracks.

Table 1
Degree of cataclasis (Types A–D) and average mesocrack density (ρ_m) obtained from three orthogonal surfaces with respect to the distance from the MTL and from the Atotsugawa Fault.

MTL - Linan route								Atotsugawa Fault - Magawa route				
No.	D (m)	Type	ρ_m	No.	D (m)	Type	ρ_m	No.	D (m)	Type	ρ_m	ρ_m
10	0	D		30	1380	B	3.6	AT1a	0.02	D	10.6	10.0
11	1	D		31	1650	B	5.0	AT1b	0.2	D	15.9	13.0
12	5	D	15.7	32	1850	A		AT1c	2	C	20.2	20.0
13	60	C/D	10.1	33	1905	B		AT1d	8	C		5.40
14	70	D		34	1910	B	4.1	AT2	20	A	5.70	4.80
15	100	C	9.2	35	2130	A	3.6	AT3	100	A	5.02	4.42
16	140	C	8.6	36	2270	A	2.7	AT4	150	A	4.68	3.94
17	180	C	6.5	37	2445	A		AT5	200	A	4.55	2.91
18	260	C/D	4.8	38	2450	A	4.5	AT6	300	A	2.23	1.93
19	330	B	5.7	39	2850	A		AT7	500	A		2.36
20	390	B/C	4.7	40	2854	A	6.0				data by Takahashi	Data by Tsutsui
21	460	B		41	2880	A	6.9					
22	500	B	4.0	42	3190	A	4.9					
23	600	C		43	3390	A						
24	690	B	2.3	44	3400	A						
25	750	C		45	3875	A						
26	860	B	3.0	46	4390	A						
27	1110	B	5.1	47	4625	A						
28	1160	A	2.8	48	5050	A						
29	1230	C		49	5200	A						

4.1.2. Measurements of mesocracks using the intercept method

Crack density was determined using the intercept method where crack interceptions were counted manually. The mesocracks show a preferred orientation, meaning that the number of intercepted mesocracks across a unit length of the counting line depends on the orientation of the line. For example, we measured the variation in crack density (with respect to the orientation of parallel counting lines) at 10° intervals for horizontal sections collected at distances from the MTL of 140 m (site 16) and 1650 m (No. 31) (Fig. 5a–c). The maximum difference in crack density for site 16 (when comparing counting lines at different orientations) is 2.5 cracks/cm, whereas for site 31 the maximum difference is 3.5 cracks/cm. Using the crack density curve with respect to the orientations of counting lines, we were able to calculate the dominant preferred orientation of mesocracks: N10° E for site 16 and N60° W for site 31. However, given that we are concerned with crack density rather than crack orientation, we prepared an orthogonal set of counting lines (relative to the original counting lines) to counter the influence of line orientation on crack density. The orthogonal set of counting lines was rotated by up to 90° and mesocracks were counted at steps of 10° (Fig. 5d–f), using the same two samples as those measured above (No. 16 and 31). The results (Fig. 5d–f) clearly indicate that mesocrack density is nearly constant with respect to the orientation of the orthogonal set of counting lines (the variation in crack density was less than 1 crack/cm), because the preferred orientation of mesocracks is fundamentally unimodal with respect to the rotation angles as shown in Fig. 5b and c, therefore the orientation difference in maximum and minimum points in these figures, for example, is just 90° and the two directions compensate each other in the orthogonal counting method to make nearly constant crack density (Fig. 5e and f). Accordingly, we adopted orthogonal counting lines to clarify the trend of mesocrack density with respect to distance from the MTL and from the Atotsugawa Fault. The influence of the spacing of mesh lines was assessed in preliminary analyses, using spacing of 50, 25, 10, 5, 2.5, and 1 mm. Compared with the crack density obtained for the finest spacing (1 mm), the deviations in crack density for spacing of 2.5 and 5 mm are less than 5%, whereas those for spacing of 10, 25, and 50 mm are up to 19%, 24%, and 38%, respectively. Consequently, we adopted a mesh with a line spacing of 5 mm. The mesh sheet of the counting area (5 × 5 cm), with a line spacing of 5 mm, was superimposed on the images using Adobe Illustrator (Fig. 6). The average number (N) of cracks per unit length, as measured along 11 horizontal and 11 vertical lines (N_X and N_Y, respectively), is given as follows:

$$N = \sqrt{N_X^2 + N_Y^2} \tag{1}$$

4.1.3. Variation in crack density within individual outcrops

To clarify whether the crack density measured in the 5 × 5 cm grid is representative of the density at larger scales, we measured the crack density in five oriented samples within 5 m of the outcrops located 140 m (No. 16) and 1650 m (No. 31) from the MTL. The difference between the maximum and minimum densities measured at each outcrop was 2.0 and 1.5 cracks/cm; thus, the range in crack density within individual outcrops is regarded to be ±1/cm.

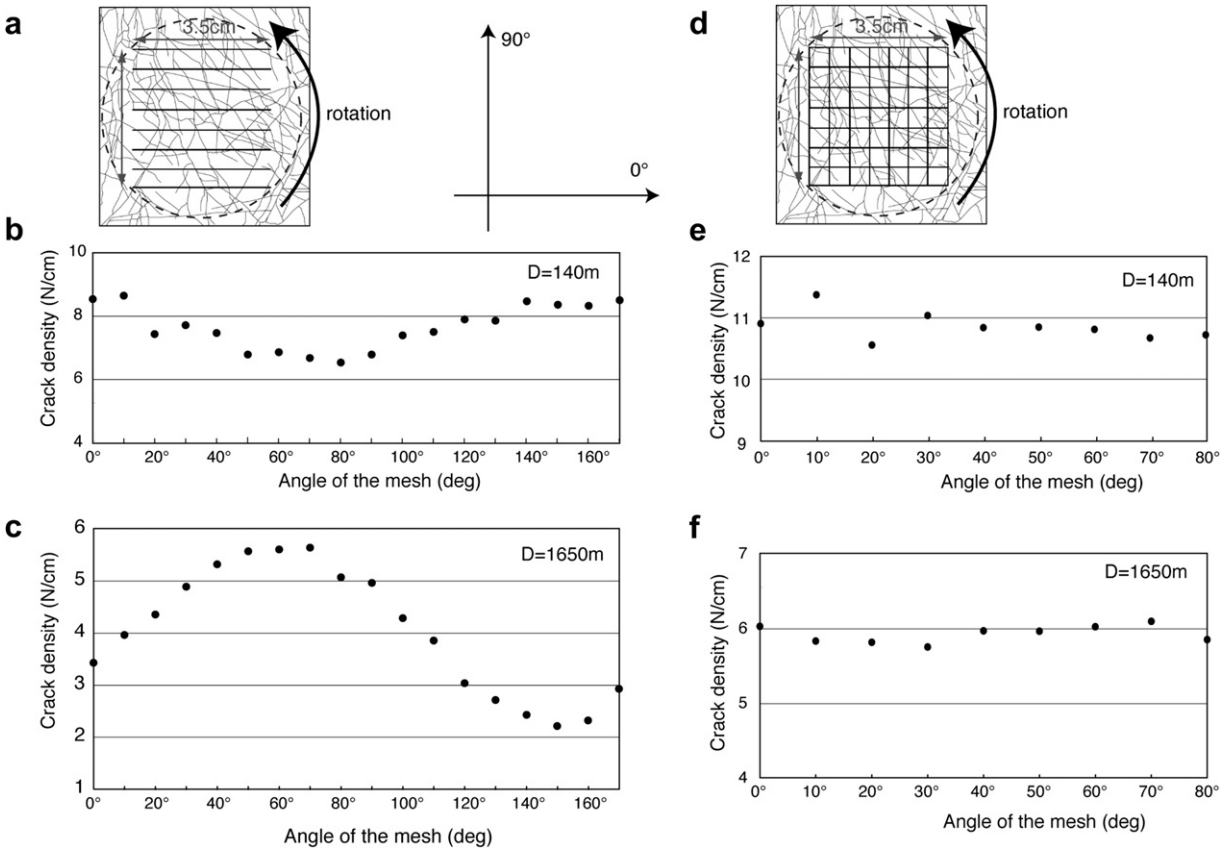

Fig. 5. Number of cracks oriented parallel (a) or across (b) arbitrary counting lines (3.5 cm in length, at a spacing of 5 mm). a. Data for parallel counting lines rotated at steps of 10°. The density of cracks varies, indicating a preferred orientation: b. Sample collected at 150 m from the MTL. c: Sample collected at 1700 m from the MTL. d. Crossed (mesh) counting lines rotated at steps of 10°. d and e: as for b and c, respectively. The number of cracks shows little change with the angle of the mesh.

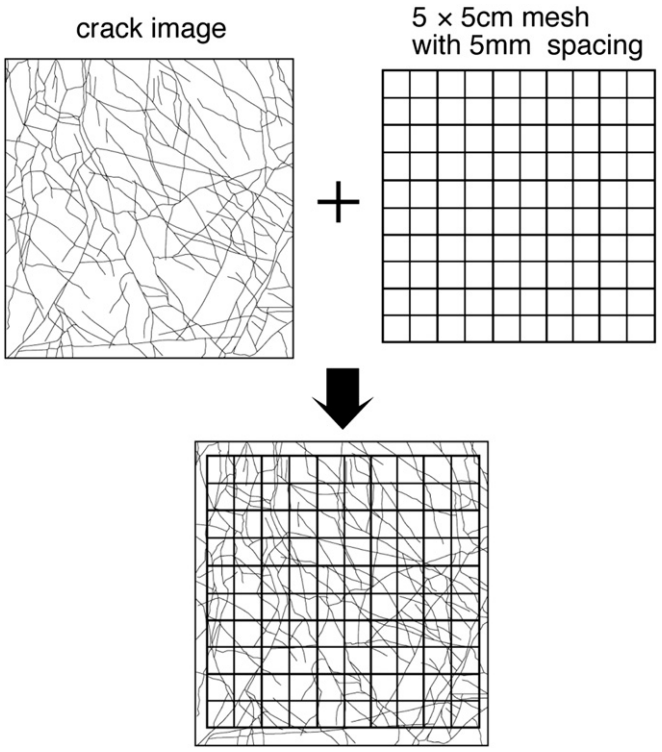

Fig. 6. Method of measuring mesocracks using a 5 × 5 cm mesh sheet (5 mm line spacing) overlain on a scanned image of the polished rock slab. We counted the number of cracks that intersected each horizontal and vertical line.

4.2. Results of measurements of mesocrack density

4.2.1. MTL: the Iinan transect

Table 1 lists data on crack density from the Iinan transect across the MTL, together with the degree of cataclasis. Fig. 7 shows photographs of selected polished slabs and corresponding line drawings of cracks, arranged with respect to distance from the MTL, while Fig. 8a shows the relationship between crack density and distance from the MTL. Among the three slabs of different orientations from which the crack densities were measured, the lowest densities were obtained for the horizontal plane. At distances greater than 500 m from the MTL, the crack density is almost constant (2–6 cracks/cm). At distances less than 500 m, the density increases when approaching the MTL, yielding a linear relationship between crack density and the logarithm of distance (dashed line in Fig. 8b). The maximum density is 14–18 cracks/cm, as obtained for the sample collected 5 m from the MTL.

4.2.2. Atotsugawa Fault: the Magawa transect

Table 1 lists the crack density data for the Magawa transect (Atotsugawa Fault), together with the degree of cataclasis. Fig. 9 shows photographs of representative polished slabs and corresponding line drawings of mesocracks, at various distances from the Atotsugawa Fault. It was difficult to collect samples of a suitable size from close to the Atotsugawa Fault (<2 m) because of their friability; consequently, only the upper surfaces of horizontal slabs were analyzed. Fig. 10 shows the relationship between crack density and distance from the Atotsugawa Fault. Within several meters of the fault, a sharp increase in crack density is seen when approaching the fault. Little difference in crack density is seen among the three orthogonal slabs from which measurements were made. The crack density is 5 cracks/cm or less (except for the sample collected at 20 m from the fault), decreasing to 2.5 cracks/cm at ~250 m from the fault; therefore, the thickness of the fault damage zone along this route is estimated to be ~250 m.

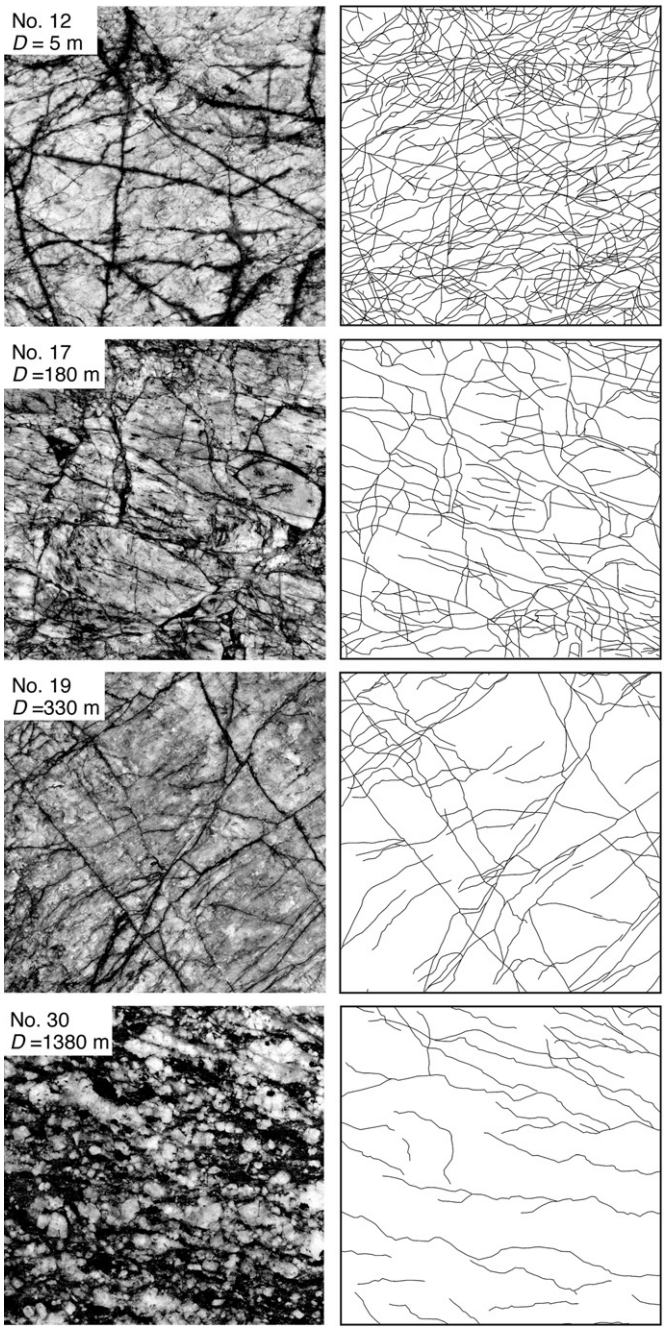

Fig. 7. Selected photographs of horizontal polished slices (left; 5 × 5 cm in size) and accompanying line drawings of cracks (Iinan transect). Samples were collected at distances from the MTL of D = 5, 180, 330, and 1380 m.

5. Analysis of intracrystalline strain using XRD

The amount of intracrystalline strain in a crystal can be measured from X-ray line broadening. We calculated the dislocation density in quartz grains from each sample along the Iinan transect at the MTL (Fig. 2) and from the Magawa transect at the Atotsugawa Fault (Fig. 3) based on X-ray line broadening, following Aikawa and Aoyama (1983). The line broadening was determined as the half wavelength (integral length) of the 110 peak. The crystallinity index

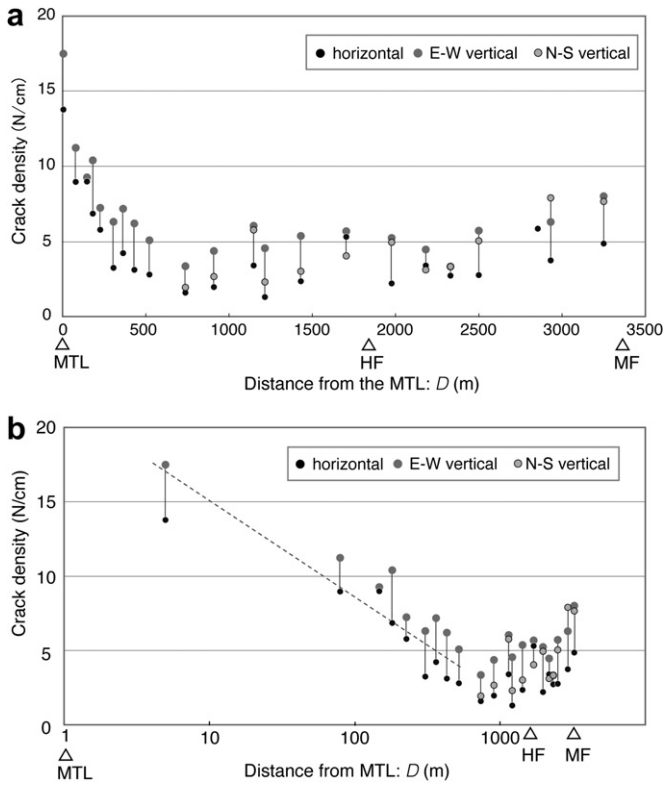

Fig. 8. Trends in mesocrack density with respect to distance (a: linear scale, b: logarithmic scale) from the MTL at the Iinan transect.

(CI) of quartz, based on the degree of resolution of the d(212) X-ray reflection peak (following Murata and Norman, 1976), was also used to assess the amount of intracrystalline strain. Takagi et al. (1988) described spatial variations in X-ray line broadening and CI across a ductile to brittle shear zone in the Ryoke belt of the Kishiwada area, Japan, revealing little variation in the transition from the protolith granite to mylonite, but pronounced X-ray line broadening and a marked decrease in CI within a sample that had endured cataclasis.

In this section, we verify whether the above results can be generalized to cataclasite, mylonite, and the protolith granite in other shear zones and faults. We also used transmission electron microscopy (TEM) to observe the dislocation substructures of quartz grains, to compare with the results of XRD analyses (line broadening and CI).

5.1. Sample preparation

Quartz powder was extracted from samples of granitic rocks (>20 g) as follows:

(1) Each sample was crushed to powder in a mill and sieved to obtain 2 g of the size fraction between #150 (105 μm) and #250 (63 μm).
(2) A solution was made by mixing the powder with phosphoric acid (H_3PO_4) and HBF_4 (for details, see Takagi et al., 1988), enabling the extraction of quartz.
(3) The quartz powder was again milled using an agate mortar and was sieved (#635; 20 μm) in water according to Stokes law to yield a 5–20 μm powder. A standard quartz powder (Brazilian rock crystal) was also prepared using the same method.

X-ray line broadening is influenced by grains of less than 1 μm in size; thus, the size fraction of 5–20 μm is suitable in terms of removing the influence of grain size on the broadening and on calculations of the CI. In ultramylonite along the MTL, the minimum grain size of recrystallized quartz is a few micrometers; accordingly, for the prepared samples, the line broadening and CI would be mainly influenced by defects in the crystal lattice, especially dislocation substructures in quartz.

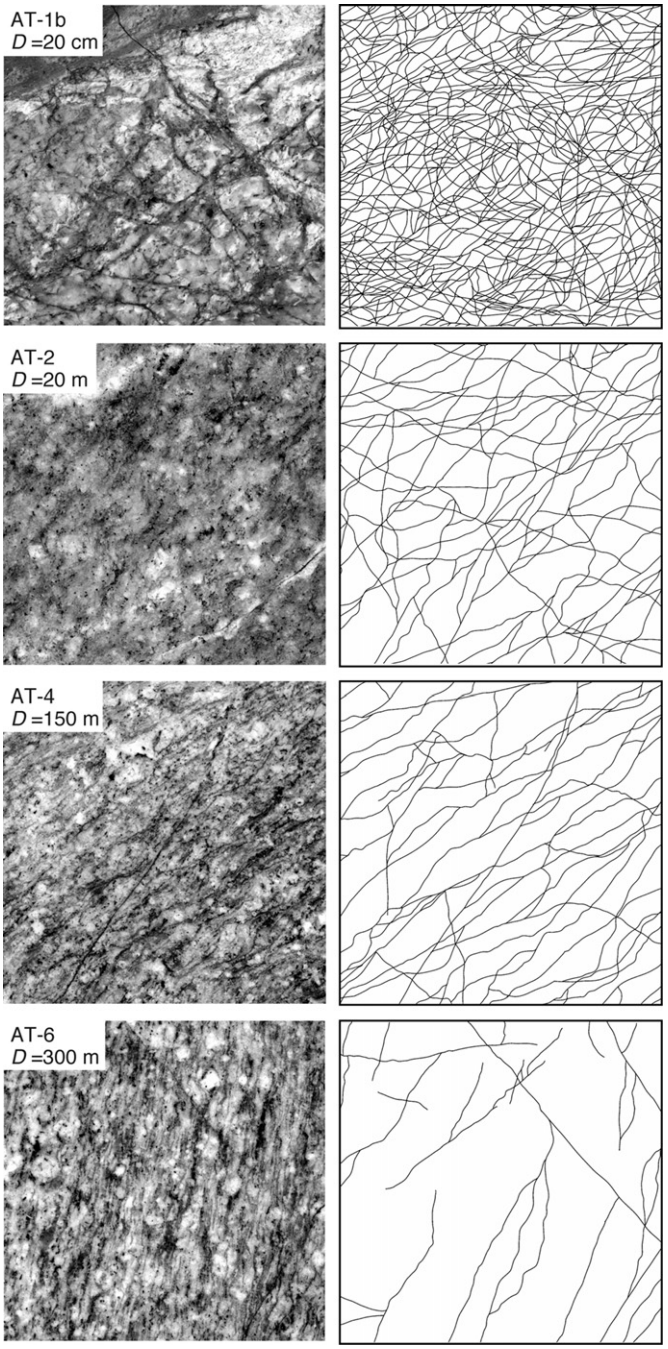

Fig. 9. Representative photographs of horizontal polished slices (left; 5 × 5 cm in size) and corresponding line drawings of cracks (traced by K. Takahashi), for samples from the Magawa transect. The samples were collected at distances from the Atotsugawa Fault of D = 20 cm, 20 m, 150 m, and 300 m.

5.2. XRD analyses

The quartz powder was placed in a glass holder with a depth of 0.2 mm and set in an XRD device (RIGAKU RAD-I, AB System)

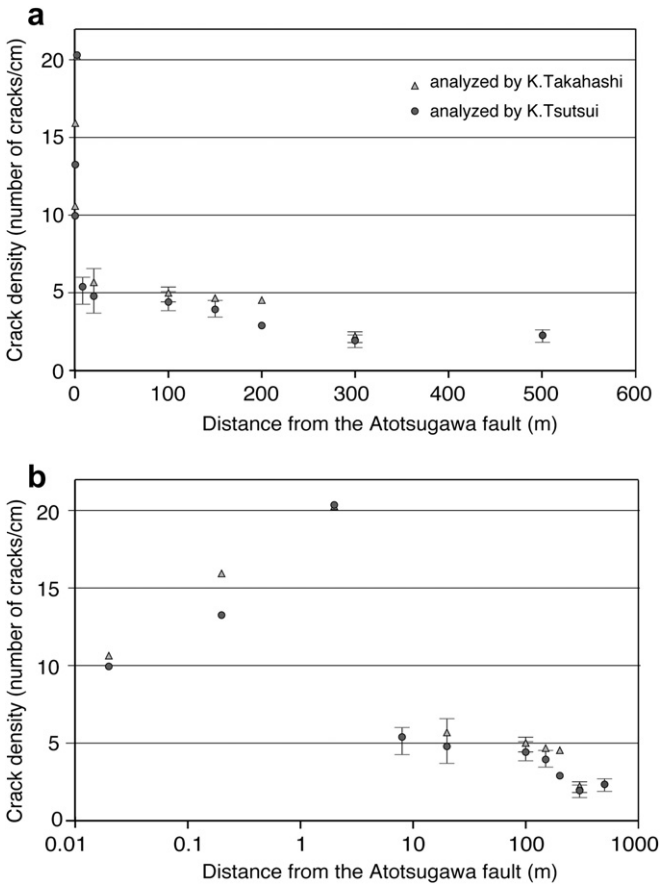

Fig. 10. Trends in mesocrack density with respect to distance (a: linear scale, b: logarithmic scale) from the Atotsugawa Fault (Magawa transect). Analytical data were measured by two students (K Takahashi and K. Tsutsui) from the same scanned images of polished slabs; both sets of data are shown for comparison. Error bars denote the range of values from three orthogonal planes from each sample (horizontal, vertical oriented N–S, and vertical oriented E–W).

housed at Waseda University, Japan. The 110 peak profile (2θ = 35.9–37.1°) for line broadening and the 212 peak profile (2θ = 66.5–69.2°) were measured using the step-scan method under analysis conditions of 40 kV and 20 mA, with nickel-filtered copper radiation. Five measurements were made of each sample, with the powder being re-mounted in the holder for each measurement. The step width and slit for the 110 profile were 0.002°/1 step, DS (divergent slit) = 1°, RS (receiving slit) = 0.15 mm, and SS (scatter slit) = 1°; for the 212 profile, the values were 0.004°/1 step (0.24°/min), DS = 1°, RS = 0.3 mm, and SS = 1°.

5.3. Results

Fig. 11 shows typical profiles of the 110 peak for line broadening and the 212 peak for CI, for both the analyzed samples and for the quartz standard. The half wavelength (B_h) and integral wavelength (B_o) are given in Fig. 11a–c. These profiles overlap with the element of $K_{\alpha 2}$; thus, only the element of $K_{\alpha 1}$ was detected using the modified Rachinger method included in the XRD system. We adopted B_o for calculating dislocation densities. B_o is derived from the intracrystalline strain β and instrumental broadening B_i. B_i was obtained from the B_o value of the quartz standard, which is assumed to be free of strain, and β was obtained using the correction curve for a low-angle reflection, following Nagao and Aikawa (1985).

The quartz standard was analyzed before and after zero-setting of the XRD instrument. Broadening related to intracrystalline strain β before and after zero-setting is given as β_A and β_B, respectively, defined as $\beta_A = 1.202B_o - 0.144$ and $\beta_B = 1.202B_o - 0.140$. CI is given as CI = 10Fa/b (Fig. 11d–f).

The average of 10 analyses of the quartz standard before and after the zero-setting (a/b) yielded the following: STD_A: $a/b = 0.680$, STD_B: $a/b = 0.691$; therefore, $F_A = 1.47$ and $F_B = 1.45$ are required to yield CI = 10 for the quartz standard.

Table 2 lists the integral breadth B_o, broadening β by intracrystalline strain, dislocation density ρ_c calculated from β (following Nagao and Aikawa, 1983), CI measurements, mean

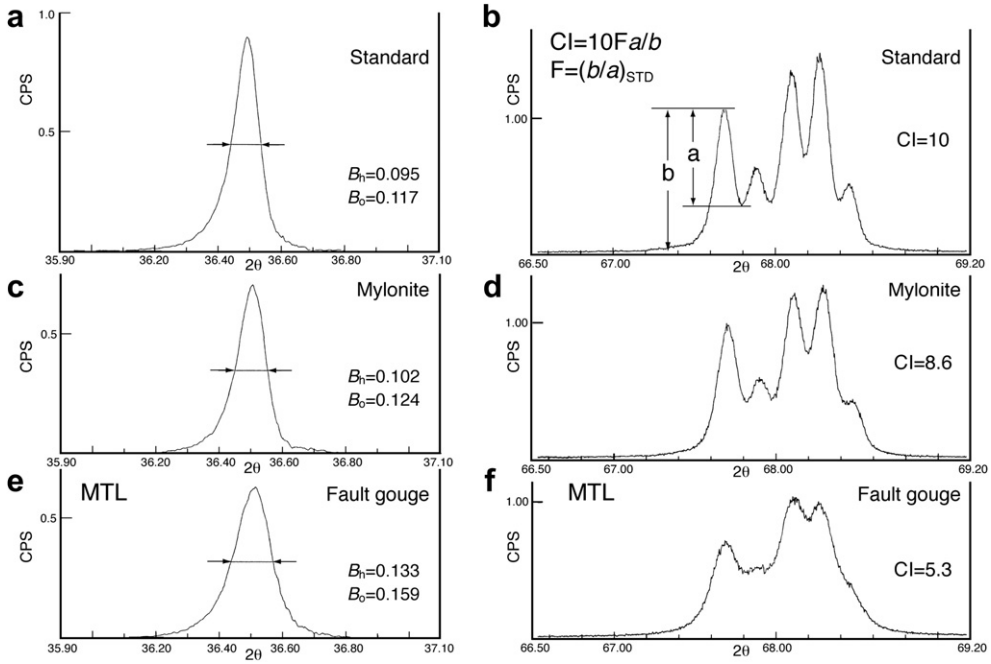

Fig. 11. Examples of line broadening at the 110 $K_{\alpha 1}$ peak (left) and the crystallinity index at the 212 peaks (right) for a Brazilian quartz standard (a, b), for mylonite samples collected at 750 m from the MTL (linan transect) (c, d), and for a sample from the margin of the MTL fault gouge, which gives the greatest line broadening and the lowest CI (e, f).

Table 2
Data on X-ray line broadening, quartz CI, grain size of recrystallized quartz, calculated and observed dislocation densities, observed dislocation length, and paleostress estimations based on grain size d (after Mercier et al., 1977) and based on dislocation density ρ_c (after McCormick, 1977).

No.	D (m)	STD	X-ray line broadening of 110		Dislocation density		Paleostress (ρ)	Quartz crystallinity index		Grain size	Paleostress (d)
			Integral breadth	Strain broadening	Calc	TEM					
			B_o (deg)	β (deg)	ρ_c ($\times 10^6$ cm^{-2})	ρ_o ($\times 10^6$ cm^{-2})	σ_ρ (MPa)	a/b	CI	d (μm)	σ_d (MPa)
Median Tectonic Line											
10	0	A	0.1594 ± 0.0014	0.0480 ± 0.0016	915		135	0.370 ± 0.011	5.43 ± 0.16		
11	1	A	0.1430 ± 0.0013	0.0282 ± 0.0015	292	126	63	0.443 ± 0.012	6.51 ± 0.17	9.9	75
13	60	A	0.1456 ± 0.0005	0.0314 ± 0.0009	365		73	0.417 ± 0.005	6.13 ± 0.07		
14	70	A	0.1458 ± 0.0012	0.0316 ± 0.0014	372		74	0.424 ± 0.015	6.24 ± 0.21		
15	100	B	0.1458 ± 0.0015	0.0351 ± 0.0018	467		86	0.438 ± 0.011	6.35 ± 0.17	9.0	80
17	180	B	0.1364 ± 0.0024	0.0238 ± 0.0029	205	90	50	0.507 ± 0.017	7.36 ± 0.24	65.5	20
19	330	B	0.1306 ± 0.0021	0.0168 ± 0.0024	98	71	30	0.573 ± 0.005	8.31 ± 0.07	62.5	20
21	460	B	0.1280 ± 0.0014	0.0137 ± 0.0017	62	48	23	0.586 ± 0.016	8.50 ± 0.23	80.1	17
23	600	B	0.1274 ± 0.0027	0.0130 ± 0.0032	58		21	0.613 ± 0.013	8.90 ± 0.19	170.4	10
25	750	B	0.1294 ± 0.0008	0.0154 ± 0.0010	79		27	0.593 ± 0.009	8.60 ± 0.12	154.0	11
29	1230	A	0.1290 ± 0.0009	0.0114 ± 0.0011	42		17	0.588 ± 0.002	8.64 ± 0.03	220.9	8
32	1850	A	0.1322 ± 0.0007	0.0188 ± 0.0009	77		26	0.568 ± 0.010	8.35 ± 0.14		
33	1905	B	0.1490 ± 0.0009	0.0389 ± 0.0010	583	211	100	0.414 ± 0.015	6.00 ± 0.22	202.7	9
37	2445									259.5	7
39	2850	A	0.1256 ± 0.0012	0.0073 ± 0.0014	17		9	0.605 ± 0.005	8.90 ± 0.07	114.9	13
43	3390	B	0.1442 ± 0.0010	0.0332 ± 0.0012	413		80	0.482 ± 0.005	6.99 ± 0.08		
44	3400	B	0.1262 ± 0.0013	0.0115 ± 0.0016	43	34	18	0.600 ± 0.009	8.69 ± 0.14	44.8	25
45	3875	A	0.1282 ± 0.0013	0.0139 ± 0.0016	35	106	15	0.586 ± 0.008	8.62 ± 0.11	107.1	14
46	4390	B	0.1296 ± 0.0005	0.0156 ± 0.0006	81		27	0.589 ± 0.010	8.54 ± 0.15	203.0	9
47	4625	B	0.1260 ± 0.0018	0.0113 ± 0.0022	42		17	0.620 ± 0.014	8.99 ± 0.20	243.3	8
48	5050	A	0.1358 ± 0.0012	0.0196 ± 0.0014	133		38	0.516 ± 0.010	7.58 ± 0.14		
49	5200									264.8	7
50	5560	B	0.1288 ± 0.0017	0.0147 ± 0.0021	72		25	0.579 ± 0.007	8.39 ± 0.10	249.8	8
Atotsugawa Fault											
AT-1a	0.02	B	0.1274 ± 0.0033	0.0130 ± 0.0039	61		21	0.629 ± 0.008	9.12 ± 0.11		
AT-1b	0.27	B	0.1250 ± 0.0011	0.0101 ± 0.0013	32		15	0.654 ± 0.013	9.49 ± 0.18		
AT-1c	2	B	0.1264 ± 0.0026	0.0118 ± 0.0031	48		19	0.626 ± 0.009	9.08 ± 0.14		
AT-2	20	B	0.1256 ± 0.0016	0.0108 ± 0.0020	38		16	0.643 ± 0.010	9.32 ± 0.15		
AT-4	100	B	0.1224 ± 0.0022	0.0070 ± 0.0027	17		9	0.643 ± 0.013	9.33 ± 0.19		
STDA			0.1194 ± 0.0034	–	–		–	0.680 ± 0.021	–		
STDB			0.1165 ± 0.0041	–	–		–	0.691 ± 0.012	–		

grain size of recrystallized quartz and calculated results of paleostress from dislocation density and from grain size. The variations in β and CI with respect to distance from the MTL and from the Atotsugawa Fault are shown in Fig. 12b and c and Fig. 13a and b, respectively. Fig. 12a shows spatial trends (with respect to distance from the MTL) in the grain size of recrystallized quartz, as an indicator of the degree of mylonitization (Takagi, 1985), to enable comparisons with the trends variations in β and CI.

5.3.1. MTL: the Iinan transect

The spatial trends in β and CI with respect to distance from the MTL are similar to each other (Fig. 12b and c), although being mirror images about a horizontal axis (cf. Fig. 14). Both sets of data are largely constant (β = 0.008–0.02, CI = 8–9) at distances of more than ~500 m from the MTL (although with some exceptions); within ~500 m of the fault, however, β and CI show marked changes toward the MTL. These trends in β and CI with respect to distance from the MTL are similar to the trend in crack density (Fig. 8a). The maximum β is 0.048 and the minimum CI is 5.4, in both cases for fault gouge upon the MTL. The dislocation density ρ_c as calculated from β, ranges from 17 to 915 $\times$ 10^6/cm^2. The paleostress σ_ρ calculated from ρ_c (after McCormick, 1977) ranges from 9 to 135 MPa.

The three anomalous data points (for distances greater than 500 m from the fault, as mentioned above) correspond to samples collected along faults characterized by cataclastic deformation (the Hiyama, Minamata, and Nyunomata faults). These spatial trends in β and CI with respect to distance from the MTL are different from the trend for the grain size of quartz (compare Fig. 12b and c with Fig. 12a), as follows: (1) the latter trend shows two peaks, near the MTL (Southern Marginal Shear Zone: SMSZ) and at 3–4 km from the MTL (Inner Shear Zone: ISZ); and (2) the reduction in grain size begins at ~1 km from the MTL. The smallest size of recrystallized quartz is about 9–10 μm, in ultramylonite located 100 m from the MTL. The ISZ shows a dextral shear sense, whereas the SMSZ, along the MTL itself, shows a sinistral shear sense. These shear zones represent the northern and southern limbs of a kilometer-scale synform; thus, the ISZ is considered to form syn- to post-mylonitization folding of the shear zones that was originally branched off from the main sinistral shear zone along the MTL (Shimada et al., 1998).

5.3.2. Atotsugawa Fault: the Magawa transect

Fig. 13a and b shows spatial trends in β and CI, respectively, with respect to distance from the Atotsugawa Fault. Both sets of values are nearly constant (β = 0.007–0.013, CI = 9.1–9.5), even for the sample (AT-1a, b, c) collected within 2 m of the Atotsugawa Fault, where the crack density is highest (11–21 cracks/cm). This trend is different from the case of the MTL (see above). Values of β and CI obtained for fault gouge and the protolith granite within 25 m of the Atera Fault (Fig. 1; a major sinistral active fault located south of the Atotsugawa Fault) are β = 0.0020–0.0099 and CI = 9.0–9.5, respectively (A. Orisaka, Waseda Univ., unpublished data).

Fig. 15 compares values of β and CI obtained for individual samples from the MTL, the Atotsugawa Fault, and the Atera Fault and the Inner Shear Zone in the Kishiwada area (Takagi et al., 1988; A. Orisaka, Waseda Univ. unpublished data). The regression line (for

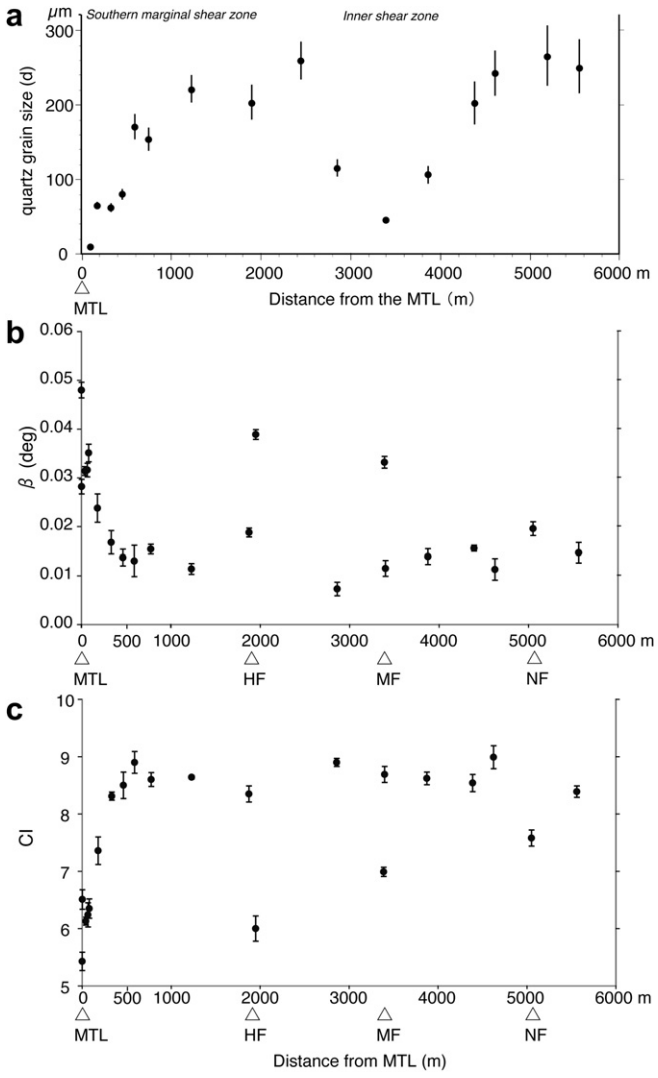

Fig. 12. Variation in the mean grain size of recrystallized quartz (a), indicating the degree of mylonitization (after Takagi, 1985), X-ray line broadening β (b), and quartz crystallinity index (c) with respect to distance from the MTL along the linan transect. HF: Hiyama Fault, MF: Minamata Fault, NF: Nyunomata Fault.

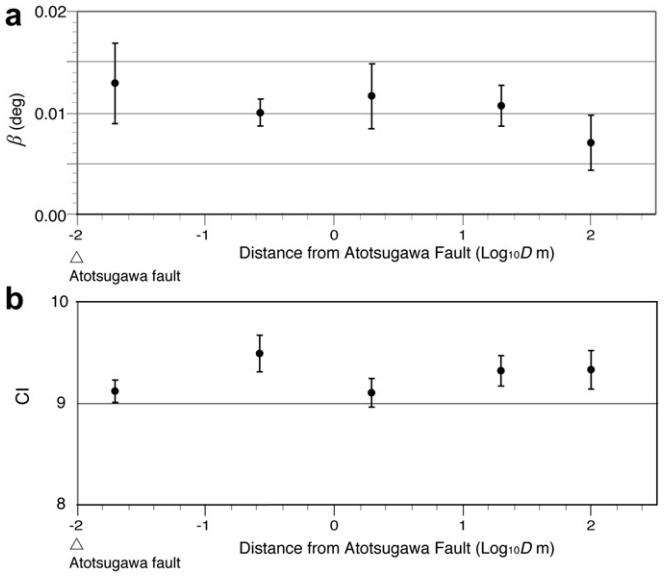

Fig. 13. Spatial trends in X-ray line broadening β and quartz crystallinity index (determined from intracrystalline strain) with respect to distance from the Atotsugawa Fault (Magawa transect).

56 data points) is as follows: CI = −98.4 β + 9.8 (regression coefficient = −0.942).

6. TEM observations of dislocations in quartz grains

The increase in β and decrease in CI when approaching the MTL is probably related to the dislocation density; consequently, we observed dislocation substructures in selected samples using TEM microscopy to determine the types of dislocation substructures that affect β and CI. We also compared the dislocation density ρ_o counted from TEM images and the density ρ_c calculated from β (Table 2). TEM observations and sample preparations using an ion thinning machine were performed at Tsukuba University.

The TEM images in Fig. 15 were selected to compare dislocations and other substructures in quartz grains in a sample from close to the MTL that underwent cataclasis after ultramylonite formation (No. 11; Fig. 15a and b), a sample of the protolith tonalite from close to the Hiyama Fault that underwent cataclasis (No. 33: Fig. 15c and d), and typical mylonitized samples (No. 17, D = 180 m, Fig. 15e; No. 19, D = 330 m, Fig. 15f). The samples shown in Fig. 15a–d were subjected to cataclasis and yield the largest values of β and the smallest values of CI (Table 2). Sample No. 11, collected close to the MTL, contains areas of short, tangled dislocations that are heterogeneously distributed (Fig. 15a), and areas of ultramylonite with newly recrystallized quartz grains (<1 μm) that show F-type substructures (Fig. 15b). Sample No. 33, collected close to the Hiyama Fault, contains areas of short, tangled dislocations that are heterogeneously distributed along microcracks, and areas of homogeneously distributed dislocations, with some short and other relatively long (Fig. 15d). The average length of dislocations in samples No. 11 and No. 33 is 0.27–0.30 μm.

Fig. 15e and f shows samples that were subjected to mylonitization but not to cataclasis. Fig. 15e shows homogeneously distributed long dislocations and “paired lobe” texture, indicating OH-bearing point defects (as well documented in experiments by McLaren et al., 1983). The average length of dislocations in samples No. 17 and No. 19 is 0.88–0.89 μm (Table 2).

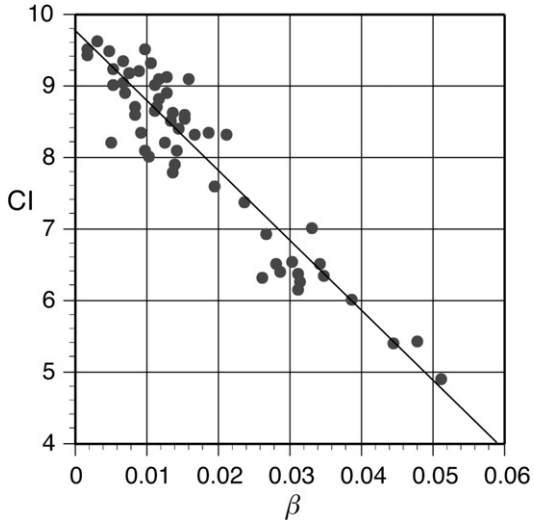

Fig. 14. Linear relationship between CI and β. Fifty-six data points are plotted, from Takagi et al. (1988), A. Orisaka (Waseda Univ. unpublished data), and the present study.

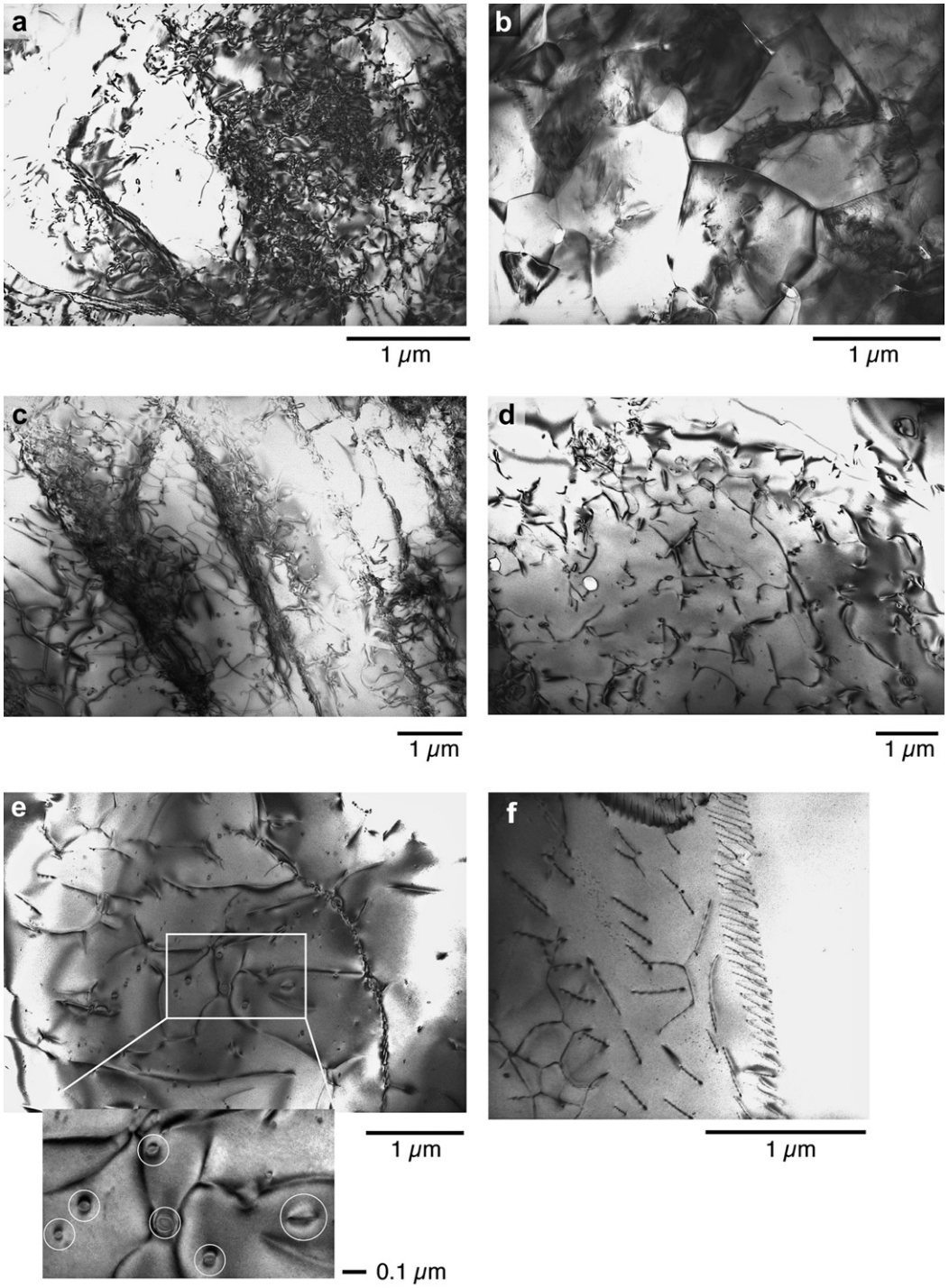

Fig. 15. TEM photomicrographs showing dislocation substructures in quartz grains. (a) Short dislocations are heterogeneously concentrated and tangled, and (b) fine-grained (1 μm) recrystallized quartz grains that characterize F-type quartz (sample No. 11 from the fault core of the MTL; distance from the fault (D) = 1 m). (c) Short dislocations are heterogeneously concentrated and tangled, producing a zonal arrangement, and (d) homogeneously distributed short and long dislocations (cataclastic sample No. 33 from along the Hiyama Fault; $D = 1905$ m from the MTL). (e) Homogeneously distributed long dislocations with OH-bearing point defects (circles in the enlargement) (mylonite containing S-type quartz; No. 17, $D = 180$ m). (f) En echelon arrangements of dislocations (mylonite containing S-type quartz; No. 19, $D = 330$ m).

The dislocation densities counted directly from enlarged images of seven samples range from 34 to 126 ($\times 10^6$ cm^{-2}). The maximum dislocation density was obtained from sample No. 33, followed by No. 11 (Table 2). These results are similar to those obtained for dislocation density ρ_c based on β, but ρ_c yields more than double the dislocation density than does ρ_o for samples No. 11, 17, and 33 (Table 2). Other samples, which were not as strongly affected by cataclasis, yield ρ_c values that are slightly larger than ρ_o, except for sample No. 45. Such large differences in values for an individual sample that underwent cataclasis are presumably attributed to the difficulty encountered in making accurate measurements of dense tangles of short dislocations from TEM images. Another possibility is that the intracrystalline strain given as β is derived not only from the dislocation density but from other

lattice defects (e.g., point defects and stacking faults) or from subdomains.

7. Discussion

7.1. Stage of the accumulation and preservation of intracrystalline strain in quartz along the MTL

Fig. 12 shows a clear difference between the spatial trend of β or CI (intracrystalline strain in quartz) and that of the grain size of recrystallized quartz with respect to distance from the MTL. Mylonitization, which is characterized by grain-size reduction of dynamically recrystallized quartz, occurs within ~1 km (Southern Marginal Shear Zone) of the MTL and also about 3–4 km (Inner Shear Zone) from the MTL and the finest quartz grain size (a few micrometers) in ultramylonite does not fundamentally affect β and CI as mentioned before, whereas abrupt changes in β and CI are observed only within ~500 m of the MTL and at close distances (within 50 m) to the other faults. In other words, the spatial trend in intracrystalline strain within quartz was developed during the cataclasis stage at a relatively shallow crustal level. Although such intracrystalline strain could also be accumulated during mylonitization at deeper crustal levels, annealing occurs simultaneous with strain at higher temperatures, meaning that dislocation tangles are not preserved during mylonitization. During the cataclasis stage, the relatively low temperatures meant that annealing was insufficient to remove tangled dislocations, resulting in a high dislocation density in quartz within cataclastic fault rocks along the MTL and other faults. Similar findings have been reported for a ductile–brittle shear zone in the Ryoke Belt within the Kishiwada area (Takagi et al., 1988), west of the Iinan area.

In estimating the paleostress σ from the grain size of recrystallized quartz, the finest grain size of P-type and S-type quartz is about 45–60 μm ($\sigma \leqq 25$ MPa), whereas that of F-type quartz in ultramylonite within 100 m of the MTL is ~9 μm ($\sigma = 80$ MPa). The dislocation density calculated from X-ray line broadening β is greatest for fault gouge from the MTL ($\rho_c = 915 \times 10^6/cm^2$), yielding a paleostress of 135 MPa. From the fabric analyses by Shimada et al. (1998), mylonitization occurred during retrograde cooling of granitic rocks, during the transition from a higher-T regime (characterized by a type-II cross girdle or *Y*-maximum fabric pattern for P-type recrystallized quartz) to a lower-T regime characterized by a type-I crossed girdle fabric pattern for P-type recrystallized quartz (<1 km from the MTL) to S-type recrystallized quartz (<200 m from the MTL). The lowest-T regime, close to the MTL (<100 m), is characterized by F-type recrystallized quartz in ultramylonite. These observations reveal that various stages of mylonitization, at different depths, are preserved at different distances from the MTL, because the ductile shear zone is wider at greater depths (i.e., the shear strain is more concentrated at shallower depths). Following the mylonitization stage, brittle deformation produced cataclasis, and pseudotachylyte was formed at ~500 m from the MTL, overprinting the mylonitic rocks at shallow crustal levels. During the final stage of cataclasis, the maximum dislocation density was formed within the fault core of the MTL, in the current fault-gouge zone. During this stage, a high dislocation density was also recorded along other faults, in addition to the MTL. TEM images of samples of the MTL fault gouge and of samples from along the Hiyama Fault reveal microcracks in the domain that contains intensely tangled short dislocations (Fig. 15a and c), suggesting that microcrack formation started to occur in the cataclasite zone, where tangled dislocations are ubiquitous, producing strain hardening.

The brittle reactivation of MTL, associated with latest generation of fault gouges and hydrothermal alteration, did not involve any significant of dislocation accumulation in quartz. The reason for this interpretation is explained in the following section.

7.2. Spatial trends in mesocrack density and evaluation of the thickness of the fault damage zone

Here, we consider spatial trends in mesocrack density with respect to distance from the MTL and from the Atotsugawa Fault. The mesoscopic crack density shows a fault-ward increase at 500 m from the MTL, suggesting that the thickness of the cataclastic zone is ~500 m. The dip of the MTL is ~60°N, indicating a true thickness is ~400 m. A similar thickness is estimated from intracrystalline strain, as β increases and CI decreases toward the MTL, starting at 500 m from the fault. The mesocrack density shows little change at distances greater than ~250 m from the Atotsugawa Fault, but shows an abrupt increase at several meters from the fault; thus, the thickness of the fault damage zone along the Atotsugawa Fault is up to 250 m.

A significant finding of this study is that the abrupt increase in crack density observed within several meters of the Atotsugawa Fault is unrelated to intracrystalline strain in quartz grains, because we observe no increase in β and no decrease in CI. This is also seen for the Atera Fault, a sinistral active fault in Central Japan (A. Orisaka, Waseda Univ., unpublished data). The difference in intracrystalline strain within quartz between the MTL and the Atotsugawa Fault suggests that the strain in quartz along the MTL was accumulated at a relatively deep crustal level (although in the brittle regime) during cataclasis, producing short, tangled dislocations. In contrast, intracrystalline strain did not occur along the Atotsugawa Fault, because the damage zone was formed at relatively shallow (brittle) levels in the crust. Mechanical energy probably resulted in fracturing without the formation of tangled dislocations along the Atotsugawa Fault. This contrast in patterns of β and CI along the MTL and the Atotsugawa Fault suggests a difference in the level within the brittle crustal levels (i.e., a difference in pressure) at which the deformation occurred. A difference in crustal level along the faults is also indicated by the contrasting thicknesses of the respective cataclastic zones.

The intensity of cataclasis was estimated qualitatively (ranked from A to D), based on microscope observations, to enable a comparison with β and CI. Using this approach, the intensity of cataclasis can be quickly determined; however, thin sections are small, meaning that the results are easily influenced by the heterogeneous distribution of fractures. Types C and D are always seen within 300 m of the MTL and within only 10 m of the Atotsugawa Fault (Table 1) consistent with the thickness of the cataclastic zone estimated from mesocrack density from both faults. Accordingly, if many thin sections are prepared over a considerable transect across a fault, information on the intensity of cataclasis is useful for evaluating the thickness of penetrative fault damage zone (or cataclastic zone). Several parasitic faults exist within 100 m of the Atotsugawa Fault (Kanaori et al., 1988), in the cataclastic zone of the shallow brittle crust; therefore, such fault zones should be taken into account when estimating the thickness of the damage zone, including non-penetrative fractures and faults. As mentioned above, the distribution of penetrative and non-penetrative cracks depends on the brittle crustal level.

The method of estimating the mesocrack density, as employed in the present study, involves the freehand tracing of cracks, which is time-consuming. It would therefore be an advantage to trace the cracks automatically, using a fluorescence method (Nishiyama et al., 1990), the replica method (Osada et al., 1999), or laser scanning microscopy for open cracks (Onishi and Shimizu, 2005). However, most of the cracks that form at depth are sealed by minerals, meaning that some manual correction might still be

required during or after automatic tracing. Using SEM-CL images for healed or sealed cracks would be another useful method to evaluate both crack density and crack area automatically (Gomez and Laubach, 2006), however, it seems applicable only for monomineralic rocks such as quartzite.

Acknowledgements

We are grateful to Prof. Nobuyuki Aikawa, Osaka City Univ., for guidance in the analytical method employed to estimate intracrystalline strain in quartz. We also thank Motoki Uehara (Railway Technical Research Institute) for assisting with XRD analyses, Dr. Norio Shigematsu (AIST) and Dr. Hiroyoshi Arai (Waseda Univ.) for fruitful discussions, and Dr. Ichiro Iwasaki (Waseda Univ.) for preparing thin sections and polished slabs. We also thank Dr. Jafar Hadizadeh and another anonymous reviewer for their constructive review on this paper.

References

Aikawa, N., Aoyama, T., 1983. Deformation of granitic rocks along the Median Tectonic line. Journal of Mineralogical Society of Japan 16 (Spec. Pub. no. 1), 251–255 (in Japanese with English abstract).

Akahane, H., Takeuchi, A., Yamamoto, S., Kunika, S., Honoki, H., 2001. Tateyama Caldera: silica Precipitation in the Shin yu Hot Spring, Erosion Control Works (Sabo) and the Atotsugawa Active Fault, 108th Annual Meeting of the geological Society of Japan, Excursion Guidebook, pp. 136–166.

Anders, M.H., Wiltschko, D.V., 1994. Microfracturing, paleostress and the growth of faults. Journal of Structural Geology 16, 795–815.

Berg, S.S., Skar, T., 2005. Controls on damage zone asymmetry of a normal fault zone: outcrop analyses of a segment of the Moab fault, SE Utah. Journal of Structural Geology 27, 1803–1822.

Chester, F.M., Logan, J.M., 1986. Implications for mechanical properties of brittle faults from observations of the Punchbowl fault zone, California. Pure and Applied Geophysics 124, 79–106.

Gomez, L.A., Laubach, S.E., 2006. Rapid digital quantification of microfracture populations. Journal of Structural Geology 28, 408–420.

Harayama, S., Takahashi, Y., Nakano, S., Kariya, Y., Komazawa, M., 2000. Geology of the Tateyama district. With geological sheet map at 1:50,000. Geological Survey of Japan, 218 (in Japanese with English abstract).

Kanaori, Y., 2001. How far does the influence of faulting extend. Journal of Japan Society of Engineering Geology 41, 323–332 (in Japanese with English abstract).

Kanaori, Y., Yairi, K., Miyakoshi, K., 1988. Deformation microstructures and their genetic process of granitic rocks in the northeastern region of the Atotsugawa fault, central Japan. Journal of the Geological Society of Japan 94, 887–901 (in Japanese with English abstract).

Kim, Y.S., Peacock, D.C.P., Sanderson, D.J., 2004. Fault damage zones. Journal of Structural Geology 26, 503–517.

Lin, A., Shimamoto, T., Maruyama, T., Sigetomi, M., Miyata, T., Takemura, K., Tanaka, H., Uda, S., Murata, A., 2001. Comparative study of cataclastic rocks from a drill core and outcrops of the Nojima Fault zone on Awaji Island, Japan. Island Arc 10, 368–380.

Masuda, T., Fujimura, A., 1981. Microstructural deformation of fine-quartz aggregates by syntectonic recrystallization. Tectonophysics 72, 105–128.

McCormick, J. W., 1977. Transmission electron microscopy of experimentally deformed synthetic quartz. PhD thesis., Univ. Calif., Los Angeles, 171 pp.

McLaren, A.C., Cook, R.F., Hyde, S.T., Tobin, R.C., 1983. The mechanisms of the formation and growth of water bubbles and associated dislocation loops in synthetic quartz. Physics and Chemistry of Minerals 9, 79–94.

Marinos, V., Marinos, P., Hoek, E., 2005. The geological strength index: applications and limitations. Bulletin of Engineering Geology and the Environment 64, 55–65.

Mercier, J.C.C., Anderson, D.A., Carter, N.L., 1977. Stress in the lithosphere: inferences from steady state flow of rocks. Pure and Applied Geophysics 115, 199–226.

Micarelli, L., Moretti, I., Jaubert, M., Moulouel, H., 2006. Fracture analysis in the south-western Corinth rift (Greece) and implications on fault hydraulic behavior. Tectonophysics 426, 31–59.

Murata, K.J., Norman II, M.B., 1976. An index of crystallinity for quartz. American Journal of Science 276, 1120–1130.

Nagao, H., Aikawa, N., 1983. Differential stress of the low P/T type Ryoke regional metamorphism, in central Kinki, Japan. Journal of Japanese Association of Mineralogy, Petrology and Economic Geology 78, 363–375.

Nagao, H., Aikawa, N., 1985. Strain and size analyses from X-ray line broadening of pulverized quartz. Journal of Geoscience, Osaka City University 28, 105–123.

Nishiyama, T., Kusuda, H., Kitagawa, M., 1990. A new method of visualization and image analysis of microcracks. Journal of Minerals and Materials Institute of Japan 106, 573–579 (in Japanese with English abstract).

Onishi, C.T., Shimizu, I., 2005. Microcrack networks in granite affected by a fault zone: visualization by confocal laser scanning microscopy. Journal of Structural Geology 27, 2268–2280.

Osada, M., Kashino, M., Yamabe, T., Yoshinaka, R., 1999. Improved method for extracting microcracks from replica film and its image analysis. Journal of Japan Society of Engineering Geology 40, 36–46 (in Japanese with English abstract).

Research Group for Active Faults of Japan, 1991. Active Faults in and around Japan: The Distribution and the Degree of Activity. University of Tokyo Press, 437 pp., in Japanese with English abstract.

Shimada, K., Takagi, H., Osawa, H., 1998. Geotectonic evolution in transpressional regime: time and space relationships between mylonitization and folding in the southern Ryoke belt, eastern Kii Peninsula, southwest Japan. Journal of the Geological Society of Japan 104, 825–844 (in Japanese with English abstract).

Shimada, K., Kobari, Y., Okamot, T., Takagi, H., Saka, Y., 2001. Pseudotachylyte veins associated with granitic cataclasite along the Median Tectonic line, eastern Kii peninsula, southwest Japan. Journal of the Geological Society of Japan 107, 117–128.

Takagi, H., 1983. Cataclastic deformation on mylonitic rocks along the Median Tectonic line - examples in Kami-Ina district, Nagano Prefecture. Gakujutu Kenkyu, School of Education, Waseda University, Series Biology and Geology 32, 47–60 (in Japanese with English abstract).

Takagi, H., 1985. Mylonitic rocks of the Ryoke belt in the Kayumi area, eastern part of Kii peninsula. Journal of the Geological Society of Japan 91, 637–651 (in Japanese with English abstract).

Takagi, H., 1986. Implications of mylonitic microstructures for the geotectonic evolution of the Median Tectonic Line, central Japan. Journal of Structural Geology 8, 3–14.

Takagi, H., Mizutani, T., Hiro-oka, K., 1988. Deformation of quartz in an inner shear zone of the Ryoke belt: an example in the Kishiwada area, Osaka Prefecture. Journal of the Geological Society of Japan 94, 869–886 (in Japanese with English abstract).

Takagi, H., Shibata, K., Sugiyama, Y., Uchiumi, S., Matsumoto, A., 1989. Isotopic ages of rocks along the Median Tectonic line in the Kayumi area, Mie Prefecture. Journal of Japanese Association of Petrology, Mineralogy and Mining Geology 84, 75–88 (in Japanese with English abstract).

Takagi, H., Iwamura, A., Awaji, D., Itaya, T., Okada, T., 2005. Dating of fault gouges from the major active faults in southwest Japan: constraints from integrated K-Ar and XRD analyses. In: Sorkhabi, R., Tsuji, Y. (Eds.), Faults, Fluid Flow, and Petroleum Traps. American Association of Petroleum Geology, Memoir, vol. 85, pp. 287–301.

Takagi, H. and Takahashi, K., 2007. New Occurrence of Pseudotachylyte from the Magawa Outcrop along the Atotsugawa Fault (Preliminary Report). Abstracts of Structural Geologists Group Meeting, Geological Society of Japan, Niigata, P-01, p. 8, in Japanese.

Takagi, H., Shimada, K., Iwano, H., Danhara, T., 2010. Oldest record of brittle deformation along the Median Tectonic Line: fission-track age for Pseudotachylyte in the Taki area, Mie Prefecture. Journal of the Geological Society of Japan 116, 45–50.

Takahashi, Y., Cho, D.-L., Kee, W.-S., 2010. Timing of mylonitization in the Funatsu shear zone within Hida belt of southwest Japan: implications for correlation with the shear zones around the Ogcheon belt in the Korean peninsula. Gondwana Research 17, 102–115.

Ui, H., Arata, S., Furuichi, S., Nishida, S., 1988. Mylonitic rocks along the Median Tectonic line near Aichi-Shizuoka Prefecture border: quartz crystallinity index and observation by SEM. Structural geology. Journal of Tectonic Research Group of Japan 33, 39–57 (in Japanese with English abstract).

Wibberley, C.A.J., Yielding, G., Di Toro, G., 2010. Recent advances in the understanding of fault zone internal structure: a review. In: Wibberley, C.A.J., et al. (Eds.), The Internal Structure of Fault Zones. Geological Society Special Publications, vol. 299.

Wilson, J.E., Chester, J.S., Chester, F.M., 2003. Microfracture analysis of fault growth and wear processes, Punchboul Fault, San Andreas system, California. Journal of Structural Geology 25, 1855–1873.